Meteoritics & Planetary Science 39, Nr 6, 799–812 (2004)
Abstract available online at http://meteoritics.org

Physical properties of rocks from the upper part of the Yaxcopoil-1 drill hole, Chicxulub crater

Y. POPOV,[1] R. ROMUSHKEVICH,[1] I. BAYUK,[1] D. KOROBKOV,[1] S. MAYR,[2] H. BURKHARDT,[2*] and H. WILHELM[3]

[1]Moscow State Geological Prospecting University, Moscow, Russia
[2]Department of Applied Geosciences, Technical University, Berlin, Germany
[3]Geophysical Institute, University Karlsruhe, Germany
[*]Corresponding author. E-mail: burkhardt@tu-berlin.de

(Received 10 September 2003; revision accepted 22 April 2004)

Abstract–Physical properties were determined in a first step on post-impact tertiary limestones from the depth interval of 404–666 m of the Yaxcopoil-1 (Yax-1) scientific well, drilled in the Chicxulub impact crater (Mexico). Thermal conductivity, thermal diffusivity, density, and porosity were measured on 120 dry and water-saturated rocks with a core sampling interval of 2–2.5 m. Non-destructive, non-contact optical scanning technology was used for thermal property measurements including thermal anisotropy and inhomogeneity. Supplementary petrophysical properties (acoustic velocities, formation resisitivity factor, internal surface, and hydraulic permeability) were determined on a selected subgroup of representative samples to derive correlations with the densely measured parameters, establishing estimated depth logs to provide calibration values for the interpretation of geophysical data. Significant short- and long-scale variations of porosity (1–37%) turned out to be the dominant factor influencing thermal, acoustic, and hydraulic properties of this post impact limestone formation. Correspondingly, large variations of thermal conductivity, thermal diffusivity, acoustic velocities, and hydraulic permeability were found. These variations of physical properties allow us to subdivide the formation into several zones. A combination of experimental data on thermal conductivity for dry and water-saturated rocks and a theoretical model of effective thermal conductivity for heterogeneous media have been used to calculate thermal conductivity of mineral skeleton and pore aspect ratio for every core under study. The results on thermal parameters are the necessary basis for the determination of heat flow density, demonstrating the necessity of dense sampling in the case of inhomogeneous rock formations.

INTRODUCTION

From geothermal investigations for the KTB (Germany) and Kola (Russia) superdeep wells (Huenges et al. 1990; Burkhardt et al. 1991; Clauser et al. 1997; Popov et al. 1999a), it was found that measurements of thermal conductivity with a spacing of 1–2.5 m are necessary to study vertical variations of geothermal parameters and to determine the terrestrial heat flow density value reliably.

Geothermal investigations performed in recent years at the Vorotilovo deep scientific well drilled in the Puchezh-Katunk impact structure (Russia) (rock thermal conductivity measured for 3715 cores) and the Noerdlingen-1973 scientific well drilled in the Ries impact structure (Germany) (rock thermal conductivity measured for 517 cores) showed certain peculiarities that may be typical of impact structures: 1) low thermal anisotropy of rocks; 2) low values of impact rock thermal conductivity in comparison with similar rocks outside impact structures that could be caused by shock-thermal metamorphism of rocks; 3) substantial vertical local variations of temperature gradient and heat flow density caused by paleoclimate and fluid motions through relatively permeable rocks of the impact structures are typical for entire section; and 4) the heat flow density in the lower parts of the impact structures was found to be lower than regional heat flow density due to the local refraction of heat flow on impact structures (Popov et al. 1998, 2000).

Therefore, numerous measurements of rock thermal properties of the cores from the Yaxcopoil-1 (Yax-1) well drilled within the Chicxulub impact crater (Dressler et al. 2003) were carried out for geothermal investigations and to study petrophysical aspects of the well section with regard to

the influence of the impact on physical properties of rocks as well as correlations between thermal and other physical properties measured in the cores and with logging methods. These correlations provide calibration values for the interpretation of geophysical data of the impact structure.

Due to an unexpected delay in sample access, the present investigation had to be restricted to the post-impact Tertiary section in the depth range of 404–666 m.

DESCRIPTION OF ROCK COLLECTION

The post-impact rocks of the Chicxulub structure presently studied are, in general, represented by tertiary limestones. The rock color varies from white, cream, and light-grey (practically without impurities) to brown, dark-brown, and grey (with impurities of iron oxide, coaly, and clayey components). The rock structure is massive, horizontal bedding (horizontal-lamination), wave-like bedding (wave-like lamination), and cross-bedding. The rock texture is mainly pelitomorphic and fine-grained. The rock-forming components of studied limestones are, in general, represented by foraminiferas; in some cases, these are longitudinal and transverse sections of *Porifera spiculas*. The size of foraminifera shells varies from 0.02 to 0.16 mm. The walls of foraminifera shells have, in general, dense microgranular texture. In particular cases, one can see radial orientation of calcite forming the shell walls. The size of *Porifera spiculas* ranges from 0.01 to 0.3 mm. Commonly, the spiculas are uniaxial and composed by silica material (chalcedony) along which calcite develops, and chalcedony of small *Poriferas* (0.01 mm) is completely replaced by calcite. The binding material consists of fine-grained or pelitomorphic calcite; some of the material is composed of neogenic calcite having greater size. In some samples (at the depths of 478.4 and 512 m), idiomorphic-grained (rhomboid) metacrystalline dolomite occurs. Impurities of black carbonaceous substance are seen in the majority of the samples, both in binding material and in rock-forming components.

A total of 120 cores recovered from the depth interval of 404.35–666.33 m have been studied in this first stage of the research. The core sampling interval was 2–2.5 m. Physical property measurements have been performed on cores with a length range of 40–80 mm. For the 120 cores, thermal properties were studied in a dry state. Only 101 cores were studied in a water-saturated state because of the danger of destroying the other 19 cores by the water-saturation procedure.

Supplementary petrophysical properties have been determined on 12 representative samples (cf., Fig. 13g) selected according to the results of thermophysical measurements.

EXPERIMENTAL METHODS

Thermophysical Properties, Density, and Porosity

Non-contact optical scanning technology was found to be best suited for geothermal and petrophysical investigations (Popov 1997; Popov et al. 1999b). The measurement procedure is described in detail in Popov and Mandel (1998).

The thermal conductivity tensor components $\lambda_{//}$ and $\lambda_{\perp}$ (parallel and perpendicular to rock bedding, respectively) and corresponding thermal diffusivity a tensor components were measured on dry samples and on samples after saturation with water. Rock saturation with water was carried out under vacuum conditions. Optical scanning allows us to record thermal conductivity and diffusivity values along each core, with the spatial resolution of λ recording about 1 cm and a recording about 1.5 cm (Fig. 1). The total errors of thermal property measurements (taking into account accuracy and

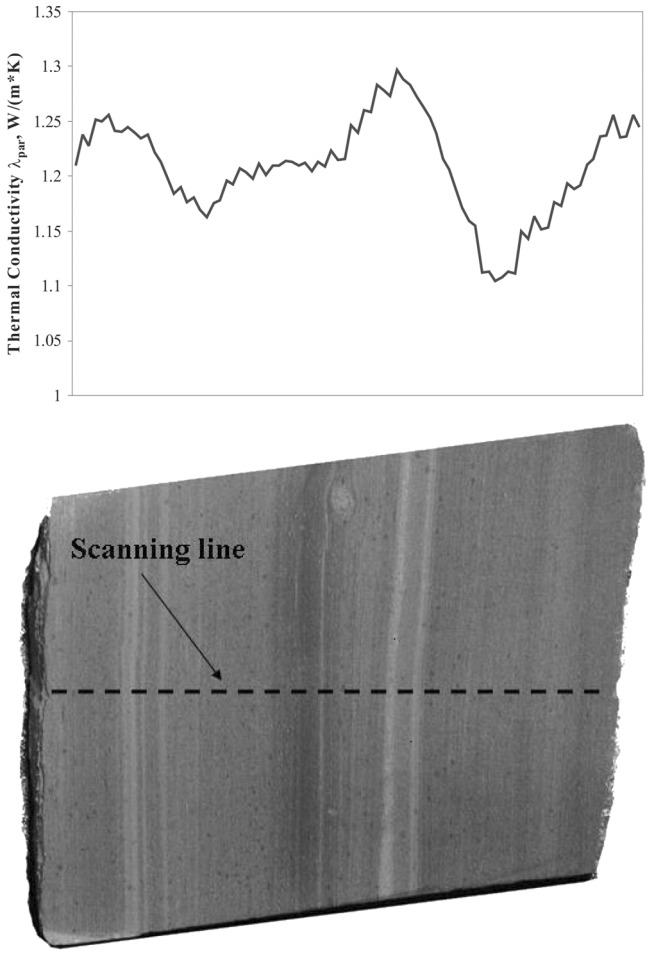

Fig. 1. Thermal conductivity profile along a dry core (sample 1394, depth 613.79 m).

precision) are about 2.5% for thermal conductivity and 4% for thermal diffusivity (for a confidence probability of 0.95) (Popov 1984).

Volumetric heat capacity $C\rho$ (where C is specific heat capacity and ρ is rock density) was determined as $C\rho = \lambda/a$, and the specific heat capacity was calculated from the formula $C = \lambda/a\rho$ after λ, a, and ρ were determined independently for dry and water-saturated samples. The anisotropy coefficient *K* was determined as $K = \lambda_{||}/\lambda_{\perp}$. The thermal inhomogeneity factor β ($\beta = [\lambda_{max}-\lambda_{min}]/\lambda_{aver}$, where λ_{max}, λ_{min}, and λ_{aver} are maximum, minimum, and average thermal conductivities recorded along each scanning line) was determined for each scanning line and for each core sample to characterize the thermal inhomogeneity of rocks (see Fig. 1).

The porosity Φ and density ρ of rock samples were determined using the water saturation method with a basic error of ±0.005 and 0.005 g/cm^3, respectively.

Supplementary Petrophysical Properties for Representative Samples

Acoustic compressional v_p and shear v_s wave velocities in dry and water-saturated samples were determined with a pulse transmission technique in the ultrasonic frequency range (0.4–1 MHz) (Wulff and Burkhardt 1996, 1997; Mayr 2002). Velocities were measured in radial and axial directions of the samples, i.e., parallel and perpendicular to the horizontal layering of the limestones. For the measurements perpendicular to layering, the samples had to be prepared. This was not possible for all 12 samples; therefore, these results are available for only seven samples. The maximum error of measured velocities is 5% in the parallel and 3% in the perpendicular direction.

The resistivity formation factor *F* (e.g., Schoen 1996) was determined for 11 samples perpendicular to layering with a four-point configuration.

The absolute internal surface S_{abs} (Schopper 1982) was measured with the BET-method (nitrogen gas) for 10 samples. The nuclear magnetic resonance (NMR) relaxation time T_2 (Kenyon 1997) was determined for six water-saturated samples. The gas-permeability *k* was measured on five samples. Due to the necessary sample size required for the measurements, permeability could only be determined perpendicular to layering. All measurements were performed under ambient conditions since, in the investigated depth range up to 660 m, the influence of pressure is expected to be rather small for the compact limestones (e.g., Schoen 1996).

EXPERIMENTAL RESULTS

Thermophysical Properties, Density, and Porosity

Thermal conductivity λ and thermal diffusivity *a* tensor components, volumetric heat capacity $C\rho$, specific heat capacity *C,* the anisotropy coefficient *K,* the thermal inhomogeneity factor β, porosity Φ, and density ρ have been determined on 120 samples from the depth interval of 404.35–666.33 m with average sampling of about 2.2 m.

The measured rock porosity ranges from 0.017 to 0.366 at an average value of 0.237. For 70% of the cores, porosity is within the range of 0.20–0.37, therefore, the studied limestones should be considered as high-porous rocks.

According to the measurement results, the thermal conductivity ranges are 0.65–2.69 W/(m · K) and 1.57–2.73 W/(m · K), the thermal diffusivity ranges are (0.69–1.44) × 10^{-6} m^2/s and (0.59–1.56) × 10^{-6} m^2/s, the volumetric heat capacity ranges are 0.94–2.01 MJ/(m^2 · K) and 1.55–3.17 MJ/(m^2 · K), and the specific heat capacity ranges are (0.57–0.88) × 10^3 J/kg · K and (0.62–1.52) × 10^3 J/(kg · K) for dry and water-saturated rock samples, respectively.

As was established earlier, the $\lambda_{||}$ component is preferable for studying correlations between λ and other physical properties (Popov et al. 2003). The experimental data (mean values for each sample [see Fig. 1 and thermal inhomogeneity factor β in Fig. 7]) from $\lambda_{||}$ for dry ($\lambda_{||d}$) and water-saturated ($\lambda_{||s}$) cores are shown in Fig. 2 together with data on solidity, which is determined as 1 − Φ, where Φ is porosity. The following peculiarities in λ data should be noted:

- Significant short-scale and long-scale variations in λ values along the section (within a range of 0.6–2.5 W/(m · K) for dry cores and 1.6–2.6 W/(m · K) for water-saturated cores; that is, up to 70% for dry and 50% for water-saturated samples relative to the average λ values);
- A coincidence in vertical variations of λ and solidity (porosity) (Fig. 3).

Three sections may be distinguished from the λ_d (dry) and λ_s (saturated) cores and porosity data from Fig. 2:

1. 404.35–533.38 m with large variations within the depth interval where the average λ_d value is $\lambda_{d\,aver}$ = 1.28 W/(m · K), $RMS_{\lambda d}$ = 0.41 W/(m · K), $\lambda_{s\,aver}$ = 1.88 W/(m · K), $RMS_{\lambda s}$ = 0.22 W/(m · K), Φ_{aver} = 25.4, and RMS_{Φ} = 0.084;
2. 533.38–576.57 m, which should be considered as relatively homogeneous with $RMS_{\lambda d}$ = 0.14 W/(m · K) at low thermal conductivity, $\lambda_{d\,aver}$ = 1.07 W/(m · K) for dry rocks, $RMS_{\lambda s}$ = 0.08 W/(m · K) and $\lambda_{s\,aver}$ = 1.72 W/(m · K), and high and stable porosity, Φ_{aver} =0.284 and RMS_{Φ} = 0.029;
3. 576.57–666.33 m, with large variations ($RMS_{\lambda d}$ = 0.40 W/[m · K] and $RMS_{\lambda s}$ = 0.25 W/[m · K]) at higher λ values ($\lambda_{d\,aver}$ = 1.62 W/[m · K] and $\lambda_{s\,aver}$ = 2.09 W/[m · K]) and lower Φ values (Φ_{aver} = 0.190 and RMS_{Φ} = 0.077). The third zone, 576.57–666.33 m, can be divided into two sub-zones with a boundary at 645 m.

Using statistical analysis based on the Wilcockson criteria χ^2, it was established that intervals (1) and (2) should be united in one zone because the difference in $\lambda_{d\,aver}$ is statistically insignificant. Zone (3) is distinguished from zones (1) and (2)

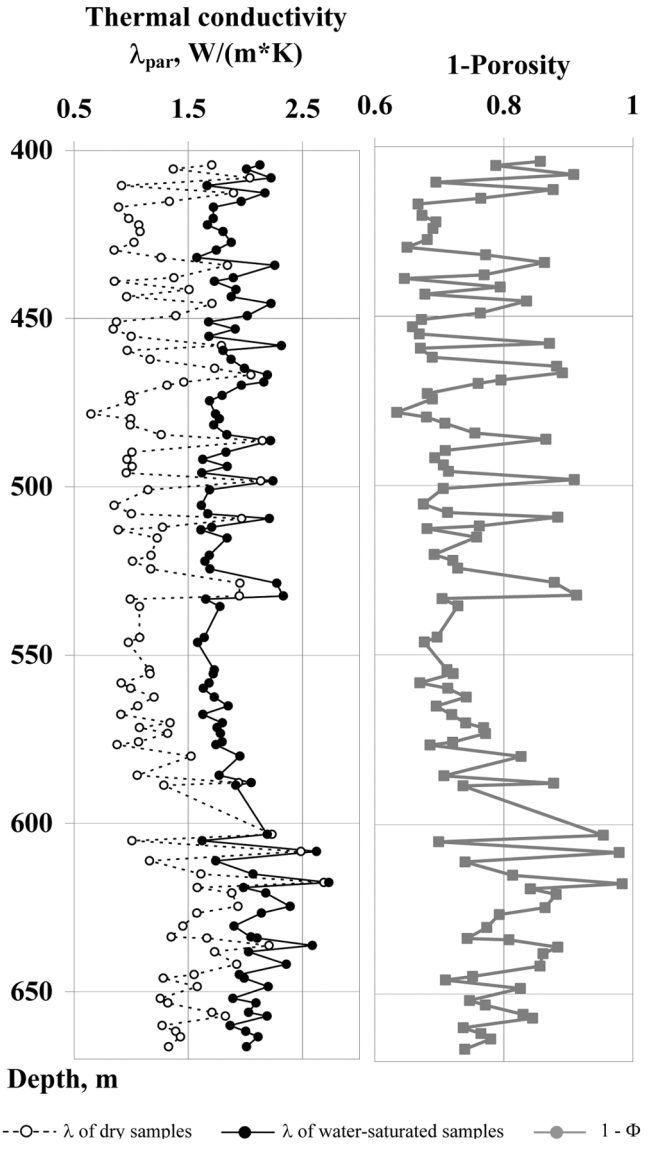

Fig. 2. Distribution of mean rock thermal conductivity λ_{par}, measured parallel to layering, and solidity (1 – Φ) along the depth section.

by $\lambda_{d\ aver}$. Statistical analysis based on the Fisher criteria (comparison RMS_λ values for two statistical groups) showed that zones (1) and (2) can be distinguished on essentially different RMS_λ values (0.41 and 0.14 W/[m · K]). Thus, zoning found from rock thermal conductivity is caused by λ variability that is connected with variations in rock porosity.

These results, as well as our previous data (Popov et al. 2002, 2003), show that variations in thermal conductivity of most types of sedimentary rocks with porosity Φ > 0.10 are caused by porosity variations when variations in mineralogical composition are of secondary importance. Fig. 3 illustrates these very close correlations between thermal conductivity for dry and water-saturated samples and porosity (correlation coefficient 0.97 and 0.86, respectively).

Experimental data on the thermal anisotropy coefficient K

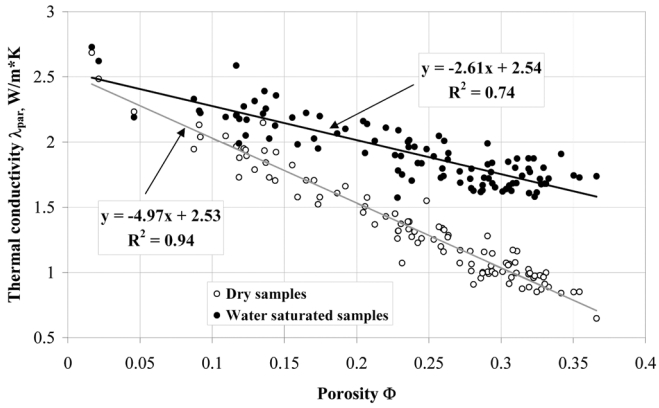

Fig. 3. Correlation between rock thermal conductivity λ_{par} and porosity Φ.

$= \lambda_{\parallel}/\lambda_{\perp}$ are shown in Fig. 4a. According to visual analysis of every core, the principal axes of thermal conductivity were chosen for the majority of samples to be oriented horizontally (sub-horizontally) and vertically (sub-vertically). Errors up to 15% in orientation cannot influence essentially the results of determination of the thermal conductivity tensor components and the anisotropy coefficient (Popov et al. 1999a). The anisotropy coefficient was found to be not very significant—no more than 1.22 for dry (1.06 on average) and no more than 1.13 for water-saturated cores (1.02 on average). A decrease in the anisotropy coefficient after the water-saturation of cores (Fig. 4a) should be explained by essential rock fracturing oriented mainly along the bedding plane. Filling open cracks with water having thermal conductivity of 0.60 W/(m · K) increases the $\lambda_{\perp}$ component more than the $\lambda_{\parallel}$ component, which leads to a decrease in the thermal anisotropy of the rock samples.

Experimental data on volumetric heat capacity $C\rho$ are shown in Fig. 4b as logs together with solidity (porosity) data. Correlations between Cρ (for dry and water-saturated cores) and porosity Φ are presented in Fig. 5. The close correlation between the Cρ of dry rocks and porosity can be explained by the high contrast in Cρ values for air and rock skeleton. In literature data on rock thermal properties, the Cρ of the rock matrix is generally assumed to be 2.23 MJ/(m^3 · K) (Beck 1988). Hartmann et al. (2003) measured heat capacity and density on 30 samples of Jurassic and older sandstones, as well as shaly sandstones, and determined the rock matrix Cρ to be (2.09 ± 0.07) MJ/(m^3 · K). From our measurements (Popov et al. 2002), we found that, in general, sedimentary rock matrix Cρ can vary substantially within the range of 1.7–2.2 MJ/(m^3 · K) and depends on the sedimentary rock type (for an example, see Fig. 5).

Experimental data on thermal diffusivity $a_{//}$ (tensor component parallel to bedding plane) are presented in Fig. 6 in correlation with corresponding λ values for dry and water-saturated cores. The data show significant variations in (a) for limestone ([0.57–1.57] × 10^{-6} m^2/s) along the section. After water-saturation, the values of λ, Cρ, and C regularly increase

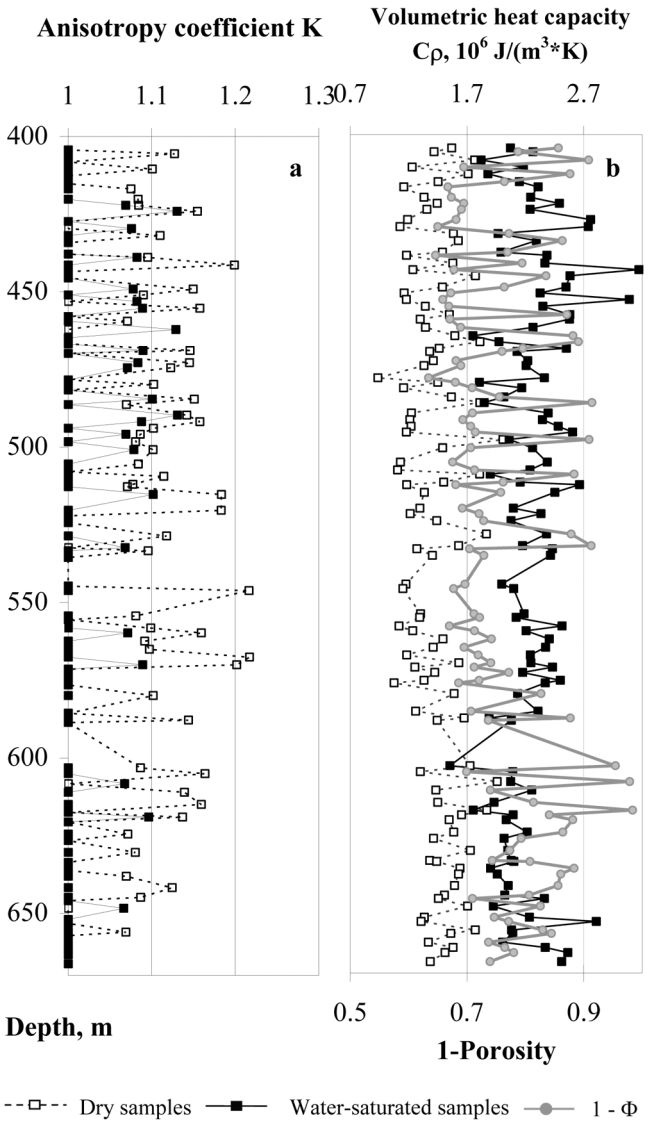

Fig. 4. Distribution of (a) the thermal anisotropy coefficient $K = \lambda_{||}/\lambda_{\perp}$ and (b) the volumetric heat capacity (Cρ) along the depth section.

by 40–55%. However, the thermal diffusivity of studied samples demonstrates a different behavior. On average, *a* decreases by 6% for water-saturated samples. Some samples exhibit an increase of up to 16%. At the same time, no change in *a* is observed for many samples after water-saturation.

From our present and previous measurements performed on many sedimentary rock collections, it can be concluded that there are typical situations with *a* variations after water-saturation: 1) for some sedimentary rock samples, *a* values increase after rock water-saturation; 2) in other cases *a* can decrease; and 3) in still other situations, *a* values are stable (within measurement accuracy).

According to theoretical modelling of rock thermal properties (see below), in our situation with the Yax-1 well, saturation of rocks with water can both decrease and increase or even leave thermal diffusivity unchanged, depending on

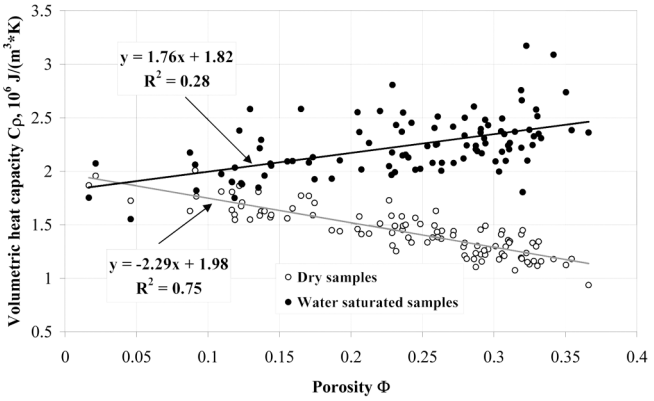

Fig. 5. Correlation between the volumetric heat capacity (Cρ) and the porosity (Φ).

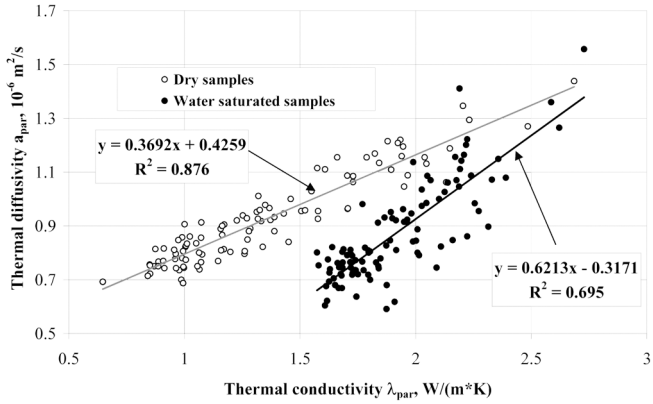

Fig. 6. Correlation between rock thermal diffusivity $a_{//}$ and thermal conductivity $\lambda_{//}$ for components parallel to layering.

the pore's aspect ratio defined for ellipsoids of revolution as the ratio of ellipsoid semi-axis along the axis of symmetry to the axis in the symmetry plane of the ellipsoid. If the aspect ratio is small (around 0.05), one can expect that the *a* values of saturated samples will be greater than the values of dry samples. For an aspect ratio around 0.1, the *a* values of saturated samples can be both greater and smaller than the *a* values of dry samples, or these values can even coincide within a porosity range. If the pores are close to spheres or have the shape of needles (aspect ratio >1), the *a* values of dry samples are greater than those of saturated samples.

The inhomogeneity factor β was determined for every scanning line on every core for the scanning direction along the bedding $\beta_{//}$ as well as for the scanning direction across the bedding $\beta_{\perp}$. Distributions of $\beta_{||}$ and $\beta_{\perp}$ along the section for dry and water-saturated cores are shown in Fig. 7. One observes much larger values of $\beta_{\perp}$ (range of 0.02–0.62 with an average value of 0.13) than $\beta_{||}$ (0.02–0.22 and 0.06, respectively).

Spatial variations in thermal conductivity along every core could, in principle, be caused by variations in: 1) mineralogical composition; 2) porosity; 3) crack density; 4)

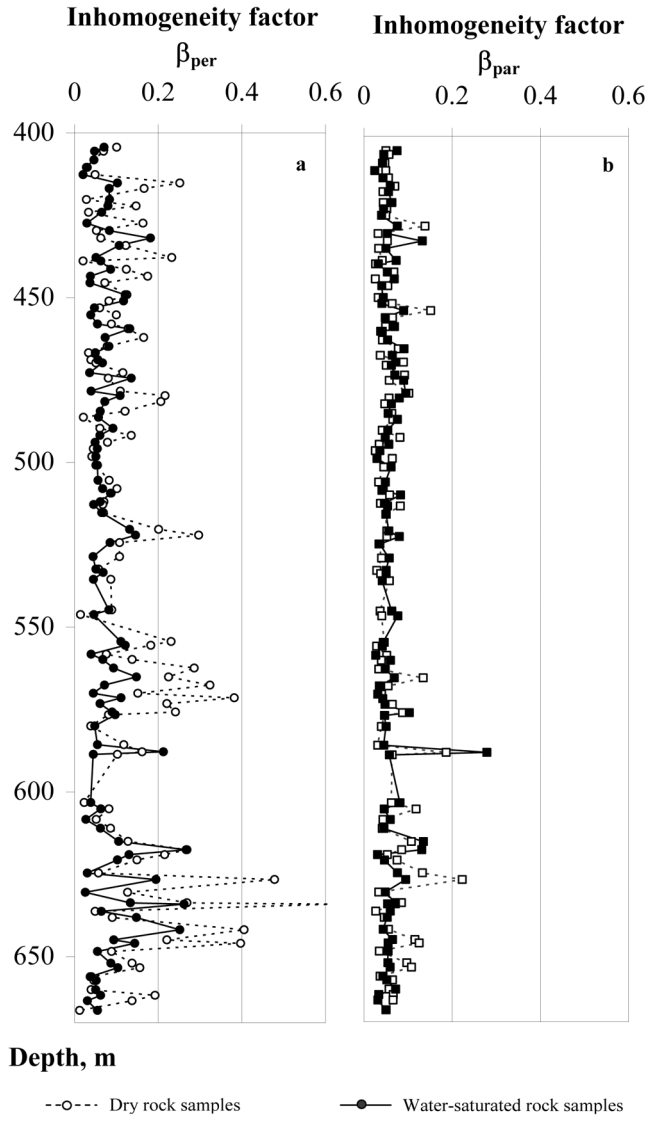

Fig. 7. Distribution of the thermal inhomogeneity factor β along the depth section.

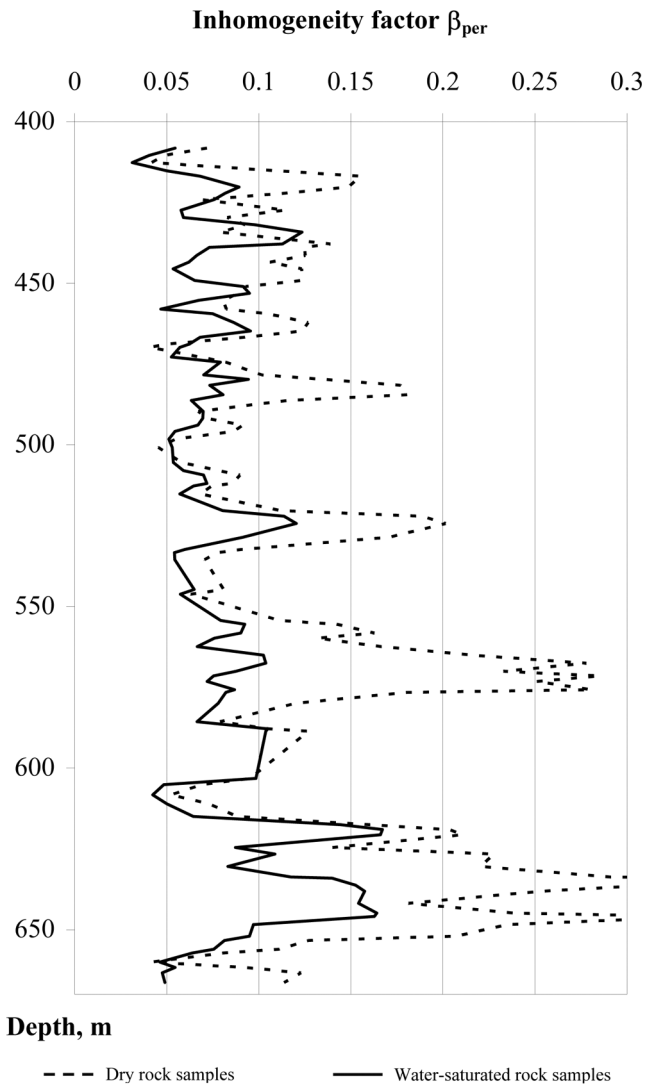

Fig. 8. Thermal inhomogeneity factor $\beta_{\perp}$, for dry and water-saturated cores processed with a box filter (3 element window).

intergrain contacts and cement material; and 5) pore and crack aspect ratio.

Three circumstances should be taken into account for the present rock collection:

1. A close correlation between thermal conductivity and porosity has been established for sedimentary dry rock collections (Popov et al. 2003) (Fig. 3).
2. An substantial decrease of $\beta_{\perp}$ occurs for most cores after their water-saturation. This is seen especially well in Fig. 8 where the $\beta_{\perp}$ range for water-saturated cores decreased up to 0.02–0.27, with an average value of 0.08 compared to 0.02–0.62 for dry cores, with an average value of 0.13, respectively (Figs. 7 and 8).
3. One observes insignificant changes in $\beta_{||}$ after water-saturation ($\beta_{||}$ ranges from 0.02–0.22, with an average value of 0.08 for dry samples and from 0.02–0.28, with an average value of 0.06 for water-saturated samples) (Fig. 7). This means that porosity variations should be considered as the principal reason for thermal inhomogeneity of rocks recorded along the cores and well. Three levels of porosity variation scales can be found from our experimental results: 1) 3–5 cm, according to thermal conductivity variations recorded along cores (single β value); 2) 5–10 m, corresponding to variations in thermal conductivity from one to the next core sample (Fig. 7); and 3) 50–70 m, corresponding to zoning in thermal conductivity variations (Fig. 7).

Supplementary Petrophysical Properties and Correlations between Parameters

The purpose of the supplementary measurements on a

selected number of representative rock samples is to derive possible correlations with the densely measured parameters of thermal conductivity, porosity, and density. These correlations, either empirical or based on theoretical models (see below), will be used to establish estimated depth logs for acoustic velocities and hydraulic permeability.

Figure 9 shows a clear negative correlation between the formation resistivity factor F and porosity Φ, in accordance with the literature ("Archie's first law"). The resulting exponent (m = –2.47 ± 0.25) is an indicator of pore morphology (e.g., tortuosity) for a specific rock type and is typical for carbonates with vugular porosity (Schoen 1996). The correlation is restricted to the porosity range from 0.08 to 0.33, omitting sample 1368 (617.53 m), which has the lowest porosity and the lowest permeability (see also Fig. 10).

The total internal surface (S_{abs}) of a sample, as measured with the BET-method (Schopper 1982), is normalized to the pore volume: $S_{por} = \rho_{dry} S_{abs}/(m\Phi)$, where ρ_{dry} is the density of the dry sample, m is the mass of the sample, and Φ is the porosity. Using nitrogen, the resolved minimum fine structure is approximately 10^{-10} m.

The correlation of S_{por} $\Phi = S_{tot}$ (specific internal surface normalized to the sample volume), with porosity Φ in the range of 0.08–0.36, shows (Fig. 10) that, for most samples, S_{tot} is approximately independent of porosity. Two samples (1377 [636.24 m] and 1391 [666.33 m]) do not fit into this correlation because of a distinctly smaller internal surface with regard to their porosity, suggesting a different type of internal structure (e.g., grain size distribution, morphology of grain surfaces).

From measured values of the formation factor F and specific internal surface S_{por}, the hydraulic permeability k was estimated using the fractal PaRiS-model (Pape et al. 1982): $\log(k) = -\log(F) - 3.1085 \log(S_{por}) + 2.6770$; (k[Darcy]).

The PaRiS-model is a further development of the standard Kozeny-Carman equation and takes the increase of internal surface by fine structures, as found in solid rocks, into account. These fine structures are modelled with generations of self-similar (fractal) geometrical structures, with the smallest structures being in the range of nitrogen atoms, as the gas used in the BET-method for the S_{por} measurements. Thus, the model takes the limited experimental resolution of the measurements into account.

The correlation of these estimated k values with thermal conductivity λ_{sat} yields a satisfactory empirical relationship between both parameters (Fig. 11). This correlation is used to derive a permeability log from densely measured thermal conductivities (Fig. 13).

The correlation between the measured acoustic velocities v_p and v_s and thermal conductivity λ is shown in Fig. 12. Since no clear systematic difference for velocities measured in parallel and perpendicular directions was found, all acoustic data are used for the correlation. The resulting linear relation between velocities and thermal conductivity is in accordance with similar empirical relations for different

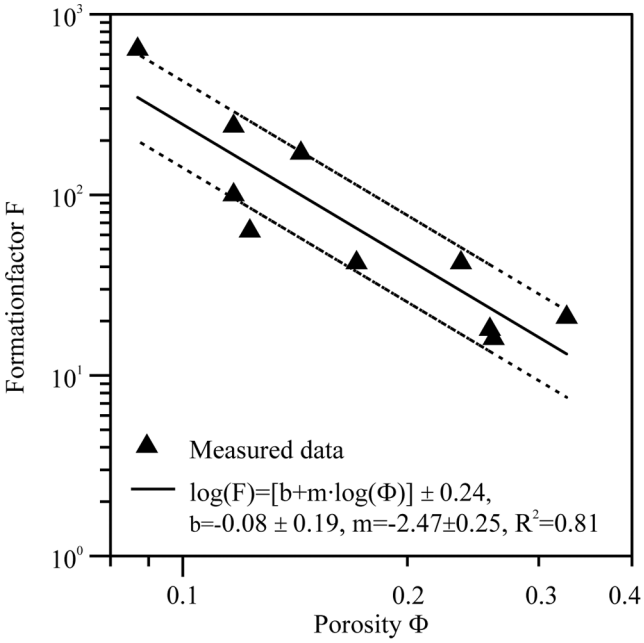

Fig. 9. Formation resistivity factor (F) in dependence with porosity (Φ). The fit log[F(logΦ)] between both parameters is restricted to the porosity range from 0.08 to 0.37. (See Figs. 13a and 13e.)

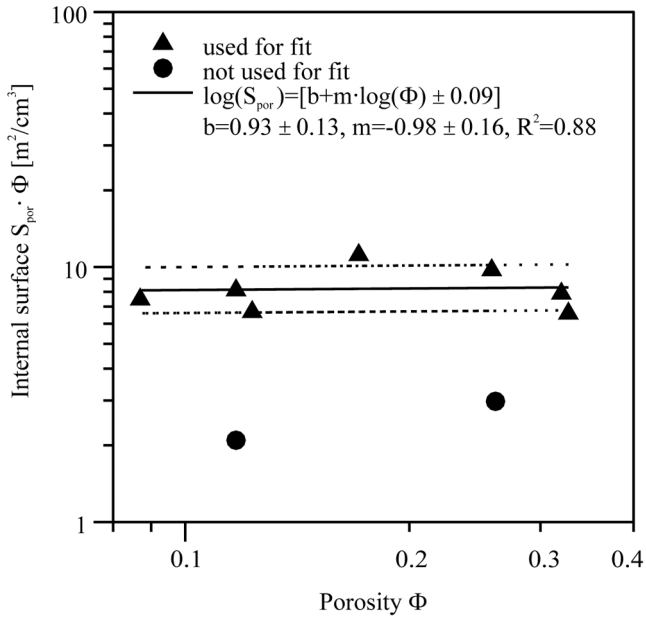

Fig. 10. Internal surface with respect to the total volume $S_{tot} = S_{por}\Phi$ in dependence with porosity Φ. The indicated correlation has the same area of validity as log[F(logΦ)] in Fig. 9. Two samples (1377 [636.42 m] and 1391 [666.33 m]) with distinctly smaller internal surface with regard to their porosity are omitted from the correlation.

rocks (Schoen 1996; Zamora et al. 1993). In the present case, this is mainly due to a similar dependence of both parameters on porosity, which is the dominant influencing factor. However, the scattering of individual values makes it clear that there are also other influences, which are different

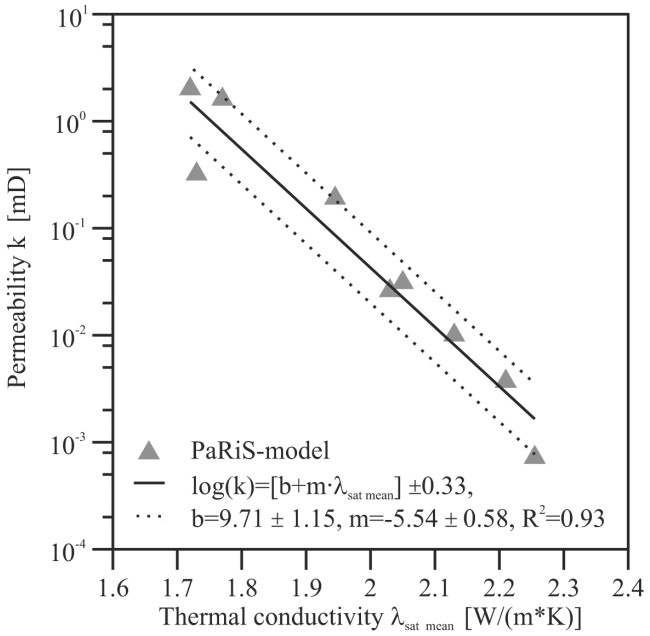

Fig. 11. Estimated permeability k (PaRiS-model) by means of measured (resp. for two values estimated from porosity; Fig. 10) specific internal surface S_{por} and formation factor F in dependence with thermal conductivity $\lambda_{sat\ mean}$ (arithmetic mean of λ_{sat} parallel and perpendicular to layering), measured under fully water-saturated conditions. Again, the fit is valid in the porosity range of $0.08 < \Phi < 0.37$.

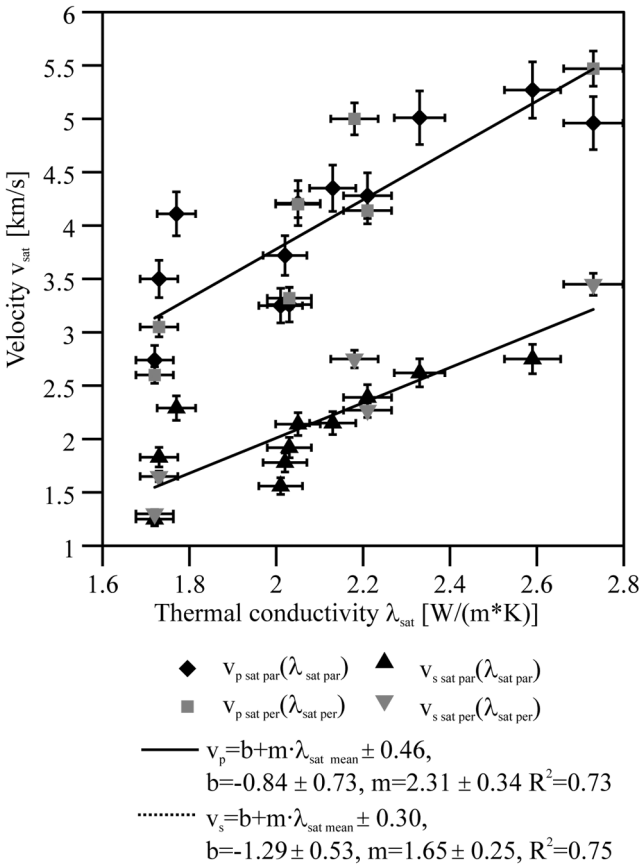

Fig. 12. Ultrasonic P and S wave velocities $v_{p\ sat}$ and $v_{s\ sat}$ in dependence with thermal conductivity λ_{sat}. For the fit, the properties measured parallel and perpendicular to layering are combined. Validity of the fit: $0.01 < \Phi < 0.37$.

for the two properties. In addition, for these inhomogeneous samples, the different experimental methods may contribute to this scattering: measured velocities are bulk values (pulse transmission method), while thermal conductivities contain information from a surface layer only (1–2 cm). Again, these correlations are used to establish estimated velocity logs from the densely measured thermal conductivities (Fig. 13).

A compilation of results for measured and estimated parameter logs is shown in Fig. 13. The matrix density log (Fig. 13b), with values generally below 2.7 g/cm^3, which is the density expected from the mineralogical composition of the limestones (95% calcite), indicates the presence of closed porosity, which is typical of carbonate rocks.

The velocity logs (Figs. 13c and 13d) are calculated from the correlation with thermal conductivity (Fig. 12). The solid symbols denote single measured values of supplementary experiments, and the lines stand for the interpolated or estimated results from dense measurement profiles of thermal conductivity. With one exception (sample 1305 [479.77 m]), there is a rather satisfactory correspondence of single measured values with the estimated logs, taking the discussion of Fig. 12 into account. This correspondence again reflects the dominant influence of porosity on both velocity and thermal conductivity for the rocks studied. Due to the large variations of porosity, acoustic velocities range from 2.7–5.3 km/s for v_p and from 1.3–3.2 km/s for v_s, with only small variations in mineralogical composition (e.g., Assefa et al. 2003).

In Fig. 13e, five different determinations of hydraulic permeability (k) are shown:

1. The black squares denote five direct measurements of k with the gas-permeameter. The permeability of sample 1368 of approximately 10^{-5} mD was at the resolution limit of the instrument.
2. The black triangles are k-estimations for six samples by NMR-measurements of relaxation time T_2: k (mD) = 0.1 Φ^4 $(T_2)^2$ (ms) (Kenyon 1997).
3. The gray triangles are estimations, calculated for individual values from formation factor (F) and specific internal surface (S_{por}), using the PaRiS-model.
4. The solid line is an estimated k-log with k = k [F(Φ), S_{por} (Φ)], using the correlations of Figs. 9 and 10 and the PaRiS-model.
5. The dashed line is an estimated k-log, using the correlation with thermal conductivity (Fig. 11).

The directly measured permeabilities for samples 1343 (562.43 m) and 1386 (656.08 m) are distinctly lower than the estimated ones. These two samples are clearly layered. Since

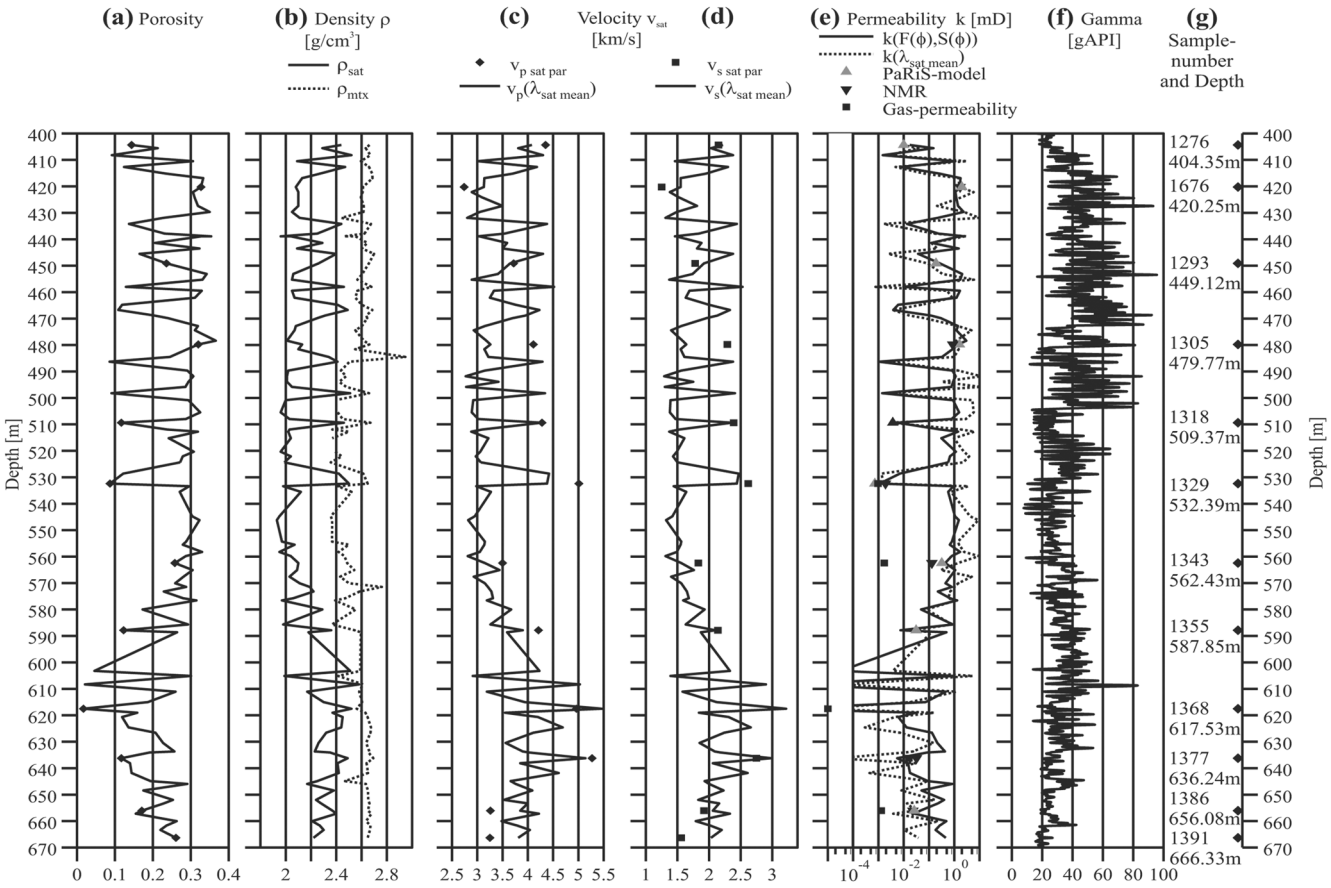

Fig. 13. Depth logs of different parameters: a) porosity; b) density of saturated rocks (ρ_{sat}) and matrix density (ρ_{mtx}); c and d) ultrasonic P wave (c) and S wave (d) velocities (fully saturated conditions) measured parallel to layering ($v_{p\ sat\ par}$ and $v_{s\ sat\ par}$) and estimated logs for the mean values $v_p(\lambda_{sat\ mean})$ and $v_s(\lambda_{sat\ mean})$ (see Fig. 12.); e) estimated permeability log from formation factor $F(\Phi)$ and $S_{por}(\Phi)$: k(F[Φ], S[Φ]), using correlations in Figs. 9 and 10 and the PaRiS-model. The estimated permeability log is from correlation with thermal conductivity: $k(\lambda_{sat\ mean})$ (see Fig. 11). The estimated permeability values are from measured S_{por} and formation factor F (PaRiS-model), as well as from NMR-T_2 measurements (NMR). The gas-permeability measured perpendicular to layering (axial direction); f) gamma log measured by the ICDP-logging team; g) sample number and depth for supplementary petrophysical measurements.

the gas-permeability could only be measured perpendicular to the layering and the estimated permeabilities are bulk values, the measured values are underestimated due to anisotropy.

In general, there is a satisfactory correspondence between the different estimations, taking the complicated nature of permeability into account. This is particularly true for the estimated values from NMR measurements and from the PaRiS-model, i.e., from two completely independent methods. Therefore, we conclude that the resulting permeability logs give at least a rough estimate of the order of magnitude for the intrinsic bulk permeabilities of the section. Again, a comparison with Fig. 13a shows a strong correlation between permeability and porosity. Nevertheless, despite very high porosities (up to 0.35) the permeabilities are, in general, below 10 mD, i.e., the tertiary limestones are characterized by large pores with only small interconnections. These small bulk permeabilities indicate that the effective hydraulic properties of this formation should be dominated by macroscopic karstic effects (see Wilhelm et al. 2004).

No clear correlation with the other logs can be seen in the gamma-log measured by the ICDP-logging team (Fig. 13f), except in the depth range of 400 m–530 m, as there are large variations in all logs.

In general, all petrophysical logs indicate that it is the porosity that dominates the physical properties rather than changes in mineral composition.

The log compilation confirms the approximate subdivision of the depth section with regard to physical properties, as seen in the thermal conductivity and porosity. From the velocity logs (Figs. 13c and 13d), an additional boundary could be identified somewhere around 600 m, marked by the transition of a relatively smooth linear increase of velocities from 3–4 km/s for v_p and 1.5–2 km/s for v_s between 570–600 m to a range of large velocity variations of 3–5.5 km/s for v_p and 1.5–3.2 km/s for v_s below 600 m.

DETERMINATION OF INTERNAL STRUCTURE OF ROCKS FROM THERMAL CONDUCTIVITIES

Theoretical Background

The experimental measurements on core samples provide thermal conductivity λ for the sample as a whole, being a macroscopic characteristic. However, each sample is microscopically inhomogeneous and consists of components having different thermal properties (mineral grains, pores, and cracks filled with different fluids). According to the definition of effective thermal conductivity, this is a tensor connecting the heat flow density and temperature gradient averaged over the sample volume. To date, many theoretical methods exist for calculating the effective thermal conductivity from the rock composition. If a rock contains components having contrasting physical properties (the case of sedimentary rocks), the methods that take the parameters of rock's internal structure into account, should be used. The most suitable theory for calculating the effective thermal conductivity of porous, cracked and, in general, anisotropic rocks is presented in Popov et al. (2003). The resulting formula includes thermal conductivity of components (the thermal conductivity of matrix and fluid filling the pores and cracks), their volume concentrations, and distribution functions of the orientation of pores and cracks in space and of the pore/crack shape. In limestones, the matrix includes mineral grains, residuals of organic material, and isolated pores/cracks. The shape of pores and cracks is assumed to be ellipsoids of revolution. In theoretical modeling, the pore/crack shape is commonly characterized by the depolarization factor. However, in practice, it is more convenient to characterize the pore/crack shape by aspect ratio: a ratio of the ellipsoid semi-axis along the axis of symmetry to the axis in the symmetry plane of the ellipsoid. The depolarization factor and pore/crack aspect ratio are related to each other by an explicit formula (Popov and Mandel 1998).

Technique of Reconstruction of the Internal Structure Parameters

We assume that cracks are ellipsoidal pores with a very low aspect ratio (less than 0.01). We called the other voids pores. Variability in the depolarization factor characterizing the pore/crack shape are described by the Beta distribution function having the parameters α and γ:

$$P(F) = \frac{\Gamma(\alpha+\gamma)}{\Gamma(\alpha)\Gamma(\gamma)} F^{\alpha-1}(1-F)^{\gamma-1} \qquad (\alpha>0, \gamma>0)$$

The mean value of F is found by:

$$m = \frac{\alpha}{\alpha+\gamma} \text{ and dispersion is: } d = \frac{\alpha\gamma}{(\alpha+\gamma)^2(\alpha+\gamma+1)}$$

This function is very flexible and, depending on the α and γ chosen, can provide different shapes, including those resembling normal, logarithmically normal, and many other distribution functions. If $\alpha = 100$ and $\gamma = 0.05$, the Beta function shape is similar to delta function and describes very thin cracks (oblate ellipsoids). If $\alpha = 4$ and $\gamma = 2$, the Beta function is related to pores. In this case, we have a mean value of F equal to 2/3, which corresponds to an aspect ratio of 0.3.

When modeling pore/crack structure, we assume that the resulting distribution function of the depolarization factor is a linear combination of the two previously mentioned distribution functions (for cracks and pores), $P_{res} = c_1 P_{crack}(F_{crack}, \alpha_1, \gamma_1) + (1 - c_1)P_{pores}(F_{pores}, \alpha_2, \gamma_2)$, i.e., we assume that the resulting distribution function can be bimodal, having maxima in the domains of cracks and pores.

Thus, we have five unknowns in the resulting distribution function. These parameters are as follows: $\alpha_1, \gamma_1, \alpha_2, \gamma_2$, and c_1. The other (sixth) unknown parameter in our modeling is the thermal conductivity of matrix $\lambda^{(matrix)}$. Hereafter, we assume that all pores and cracks are randomly oriented in space, which results in isotropic effective thermal conductivity.

The previously mentioned six unknowns are found from the minimization of the functional, which is a sum of squared relative residuals between experimental and theoretical values of effective thermal conductivity when saturating with N different fluids having contrasting thermal conductivity. The values $\lambda^{(matrix)}$, α_1, γ_1, α_2, γ_2, and c_1, providing the minimum of functional, are the solution to the problem. Since, as a rule, N = 3 or even N = 2 in experimental study of samples, i.e., we have three or two types of saturating fluids, but the number of unknowns is six, we should use all a priori information to find the parameters that provide a minimum in a physically reliable domain. Thus, information on mineral composition is rather valuable because it allows one to set a proper initial value of matrix thermal conductivity. To determine the initial approach to the Beta function parameters, it is useful to solve a similar inverse problem for determining a single aspect ratio of pores (i.e., for the case when the distribution function is a delta function), which gives information on the dominant pore shape. If thin sections are available for a collection, they can provide preliminary knowledge on the distribution function character.

Results of the Determination of the Internal Structure of Rocks

Since the majority of the studied rock samples exhibits isotropic or only slightly anisotropic thermal properties, we apply the previously mentioned technique to find the internal structure parameters.

Minimization of the functional for the rock samples with an initial approach and with bounds for sought-for parameters, chosen as varying in a physically reliable domain, gives the following averaged relative deviation between experimental and theoretical thermal conductivity values,

calculated with optimum parameters: 0.05% for dry samples and –0.05% for water-saturated samples. The maximum deviations are 2.2% and –2.3% for dry and saturated samples, respectively. Note that, for optimization, we use the thermal conductivity component $\lambda_{//}$ (Popov et al. 2003).

The thermal conductivity values of matrix found from the inverse problem solution vary, in general, between 2.3 to 2.8 W/(m · K), averaging 2.58 W/(m · K), which corresponds well to the extrapolation of experimental results to zero porosity (Fig. 3). No specific depth intervals in the behavior of the thermal conductivity of matrix are revealed. The fact that this value is smaller than that of calcite (3.2 W/[m · K]) despite the fact that the samples consist of about 95% calcite can be accounted for by the following factors. According to literature data (Amyx et al. 1960), carbonate rocks can contain closed porosity that decreases the thermal conductivity of matrix. Another factor is related to the quality of contacts between mineral grains. The weaker the contacts, the smaller the matrix thermal conductivity.

The parameters of the Beta distribution functions, determined with the proposed technique, indicate that, in general, the samples have stable pore/crack structure over the whole depth range studied. Note that, for all samples, the parameter c_1 is found to be 0, i.e., the distribution function has a unimodal character. Figure 14 shows the distribution functions over the pore/crack aspect ratio that are typical of the three previously mentioned depth intervals. The distribution functions have a maximum aspect ratio of about 0.1–0.2 with long tails in the domain of thinner cracks (up to an aspect ratio of 10^{-3}–10^{-4}). Pores having the shape of prolate ellipsoids (aspect ratio >1) with aspect ratios varying from 1 (spherical pores) to 3 can be also observed. At first glance, the three distribution functions shown in Fig. 14 have similar shapes. However, one can observe that samples from the second zone (533.38–576.57 m) exhibit stable enhanced porosity and are characterized by thinner cracks compared to the other zones. This fact can also contribute (together with enhanced porosity) to the decrease in the measured thermal

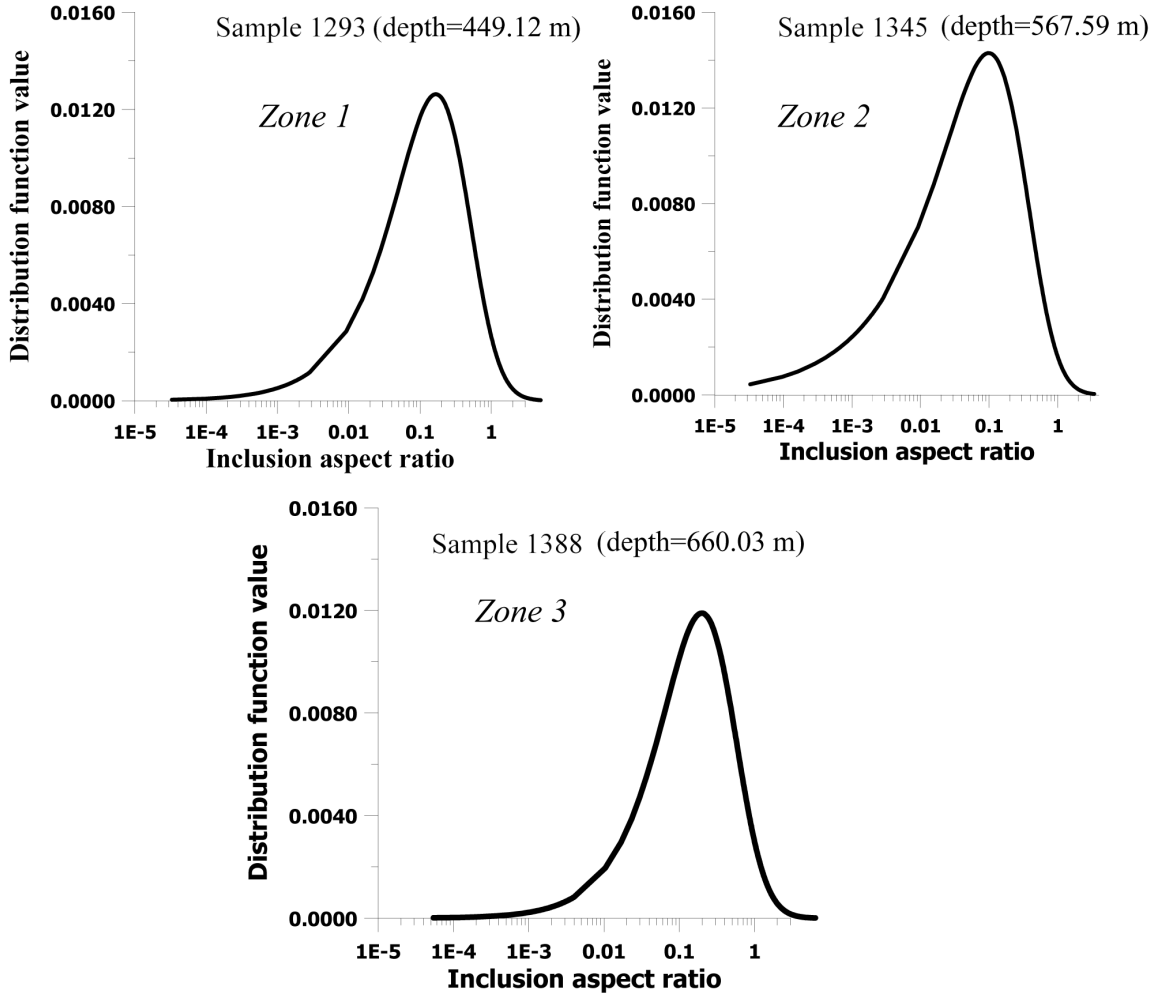

Fig. 14. Examples of distribution functions over pore/crack aspect ratios found for the three depth intervals (zones) revealed. Zone 1: 404–533 m; zone 2: 533–577 m; zone 3: 577–666 m.

conductivity values because, according to the theoretical models, the thinner the cracks at a given porosity, the smaller the calculated values of thermal conductivity. The third zone (576.570–666.23 m) is characterized by less-fractured rocks compared to the other zones.

Figure 15 shows images of thin sections of limestone samples and the related distribution functions over the pore/crack aspect ratio determined with the proposed technique. The grey, fine-grained mass is calcite, and the black color shows pores and fractures. Image (a) corresponds to the

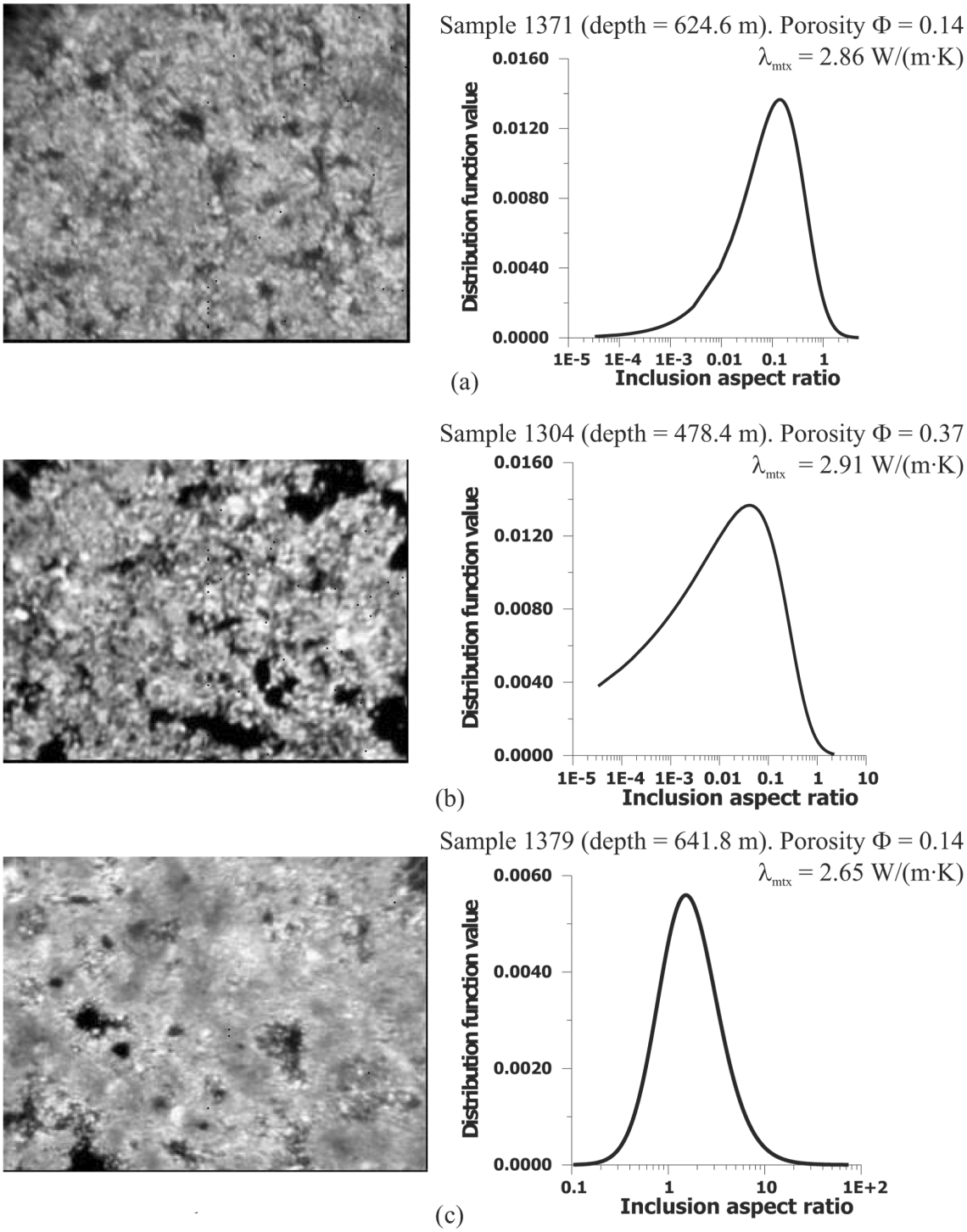

Fig. 15. Thin section photos and related distribution functions found for characteristic rock samples.

typical case of distribution function shape (α is around 4, and γ is around 2). Images (b) and (c) are related to uncommon cases of distribution functions. One can conclude that the shape of the distribution functions found from the inverse problem solution is in good correspondence with the structure seen in the images. Thus, open pores are well-seen in images (a) and (b). However, sample (b) seems to be more fractured. This fact is reflected by the enhanced value of the distribution function of sample (b) in the domain of thin cracks. Image (c) shows a sample with spherical pores. The related distribution function has a maximum around 1.5 and indicates that the aspect ratio cannot be smaller than 0.1, i.e., this sample is not fractured.

CONCLUSIONS

1. Sedimentary rocks from the upper part of the Yax-1 drill hole are characterized by significant short- and long-scale variations in thermal properties as well as in acoustic velocities and hydraulic permeability. These strong variations in thermal properties have to be taken into account in the interpretation of borehole-temperature logs, impeding the determination of heat flow density (see Wilhelm et al. 2004). On the other hand, these results demonstrate the necessity for the dense sampling of thermal rock parameters for reliable heat flow determinations.
2. Short- and long-scale variations in thermal conductivity of rocks established along the section and along the core samples are caused mainly by spatial variations in rock porosity. The same is true for acoustic velocities and for hydraulic permeability throughout the section.
3. For rocks with an essential thermal anisotropy coefficient (up to K = 1.22), the anisotropy effect should be explained basically by oriented fracturing of rock samples.
4. From supplementary petrophysical measurements on selected representative samples, estimated depth logs for acoustic velocities and for hydraulic permeability were established by correlation with densely measured thermal conductivity, density, and porosity. All logs can be used as input parameters for the interpretation of various geophysical data (e.g., geothermal, seismic, and gravity data). This is especially important in depth sections, where the petrophysical borehole logs are not available, as is the case in the depth range under study.
5. The studied thermal conductivity of rock matrix, determined as the inverse problem solution based on thermal conductivity measurements on dry and water-saturated samples, is found to vary from 2.3 to 2.8 W/(m · K), averaging 2.58 W/(m · K).
6. In general, the shape of the distribution function over the pore/space aspect ratio remains rather stable in the whole range of the studied depth interval. The aspect ratio maximum is observed around 0.1–0.2, with a long tail toward thin cracks (aspect ratio up to 10^{-3}–10^{-4}). Cracks having the shape of prolate ellipsoids are also observed, which have an aspect ratio no greater than 3. However, the three revealed depth zones exhibit specific features in the distribution function behavior. Thus, the second zone, having stable enhanced porosity, mainly contains the rocks being most fractured compared to other zones. The least-fractured rocks are observed in the third zone.
7. The same experimental procedure and interpretation strategy will be followed for the impact and pre-impact section of the Yax-1 drill hole.

Acknowledgments–The research was funded by the Deutsche Forschungsgemeinschaft (DFG grant BU 298/16) within the Chicxulub ICDP-project. The authors also wish to acknowledge support from Schlumberger Oilfield Services (an international company in the oil and gas industry). The authors thank Dr. H. Urrutia and Dr. A. M. Soler from UNAM (Mexico) for their help in core collection, preparation, and delivery, A. Pakhomov (from MSGPU) for his active help in thermal property measurements, U. Trautwein (GFZ Potsdam) for permeability measurements, and J. Urrutia and J. Šafanda for helpful comments.

Editorial Handling—Dr. Jaime Urrutia-Fucugauchi

REFERENCES

Amyx J. W., Bass D. M., and Whiting R. L., Jr. 1960. *Petroleum reservoir engineering. Physical properties.* New York: McGraw-Hill. 570 p.

Assefa S., McCann C., and Sothcott J. 2003. Velocities of compressional and shear waves in limestones. *Geophysical Prospecting* 51:1–13.

Beck A. E. 1988. Methods for determining thermal conductivity and thermal diffusivity. In *Handbook on terrestrial heat flow density determination,* edited by Haenel R., Rybach L., and Stegena L. Dordrecht: Kluwer. pp. 87–124.

Burkhardt H., Erbas K., Giese P., Haack U., Honarmand H., Huenges E., Stiefel A., Wilhelm H., Zoth G., Buntebarth G., and Schulz R. 1991. The measured and the predicted temperature profile in the KTB pilot-hole. *Scientific Results/Proceedings of the Ocean Drilling Program (Scientific Drilling)* 2:224–257.

Clauser C., Giese P., Huenges E., Kohl T., Lehmann H., Rybach L., Safanda J., Wilhelm H., Windloff K., and Zoth G. 1997. The thermal regime of the crystalline continental crust: Implications from the KTB. *Journal of Geophysical Research—Solid Earth* 102:18417–18441.

Dressler B. O., Sharpton V. L., Morgan J., Buffler R., Moran D., Smit J., Stöffler D., and Urrutia J. 2003. Investigating a 65 Ma-old smoking gun: Deep drilling of the Chicxulub impact structure. *Eos Transactions* 84:125.

Hartmann A., Rath V., and Clauser C. 2003. Thermal conductivity from core and well log data (abstract #06667). Geophysical Research Abstracts. EGS-AGU-EUG Joint Assembly 5. CD-ROM.

Huenges E., Burkhardt H., and Erbas K. 1990. Thermal conductivity profile of the KTB pilot corehole. *Scientific Results/Proceedings of the Ocean Drilling Program (Scientific Drilling)* 2:224–230.

Kenyon W. E. 1997. Petrophysical principles of application of NMR logging. *Log Analyst* 38:21–43.

Mayr S. 2002. Der Einfluss der Mikrostruktur auf die Ultraschalleigenschaften von Sandsteinen bei hydrostatischen Druckbedingungen (The influence of the microstructure on the ultrasonic behavior of sandstones under hydrostatic pressure). Ph.D. thesis, Technical University of Berlin, Berlin, Germany.

Pape H., Rieper L., and Schopper J. R. 1982. A Pigeon-hole model for relating permeability to specific surface. *Log Analyst* 23:5–13.

Popov Y. 1997. Optical scanning technology for nondestructive contactless measurements of thermal conductivity and diffusivity of solid matters. In *Experimental heat transfer, fluid mechanics and thermodynamics.* Proceedings of the 4th World Conference. pp. 109–117.

Popov Y. 1984. Theoretical models of the method of determination of the thermal properties of rocks on the basis of movable sources. *Geologiya i Razvedka* 2:83–86. In Russian.

Popov Y. and Mandel A. M. 1998. Geothermal study of anisotropic rock masses. *Izvestiya, Physics of the Solid Earth* 34:903–915.

Popov Y., Pimenov V. P., Pevzner L. A., Romushkevich R. A., and Popov E. A. 1998. Geothermal characteristics of the Vorotilovo deep borehole drilled into the Puchezh-Katunk impact structure. *Tectonophysics* 291:205–223.

Popov Y., Pevzner S. L., Pimenov V. P., and Romushkevich R. A. 1999a. New geothermal data from the Kola superdeep well SG-3. *Tectonophysics* 30:177–196.

Popov Y., Pribnow D., Sass J., Williams C., and Burkhardt H. 1999b. Characterisation of rock thermal conductivity by high-resolution optical scanning. *Geothermics* 28:253–276.

Popov Y., Pohl J., Romushkevich R., Tertychnyi V., and Soffel H. 2000. Geotermicheskiye kharakteristiki impaktnoy struktury Riis (Germaniya). In *The Earth's thermal field and related research methods,* edited by Khutorskoy M. Moscow: RPFU Publications. pp. 99–106. In Russian.

Popov Y. and Romushkevich R. 2002. Thermal conductivity of rocks of oil-gas fields. Proceedings, International Conference "The Earth's Thermal Field and Related Research Methods. pp. 219–223.

Popov Y., Korobkov D., and Miklashevskiy D. 2002. Thermal diffusivity measurements: New experimental data and theoretical background and results. Proceedings, International Conference "The Earth's Thermal Field and Related Research Methods. pp. 214–218.

Popov Y., Tertychnyi V. V., Romushkevich R. A., Korobkov D. A., and Pohl J. 2003. Interrelations between thermal conductivity and other physical properties of rocks: Experimental data. *Pure and Applied Geophysics* 160:1137–1161.

Schoen J. H. 1996. *Physical properties of rocks: Fundamentals and principles of petrophysics,* 1st ed. Oxford: Pergamon Press. 583 p.

Schopper J. R. 1982. Porosity and permeability. In *Landolt-Boernstein, group V geophysics, volume 1, subvolume A,* edited by Angenheister G. New York: Springer-Verlag. pp. 184–303.

Wilhelm H., Heidinger P., Šafanda J., Čermák V., Burkhardt H., and Popov Y. 2004. High resolution temperature measurements in the borehole Yaxcopoil-1, Mexico. *Meteoritics & Planetary Science.* This issue.

Wulff A. M. and Burkhardt H. 1996. The influence of local fluid flow and the microstructure on elastic and anelastic rock properties. *Surveys in Geophysics* 17:347–360.

Wulff A. M. and Burkhardt H. 1997. Mechanisms affecting ultrasonic wave propagation in fluid-containing sandstones under high hydrostatic pressure. *Journal of Geophysical Research—Solid Earth* 102:3043–3050.

Zamora M., Thanh D. V., Bienfait G. P., and Poirier J. P. 1993. An empirical relationship between thermal conductivity and elastic wave velocities in sandstone. *Geophysical Research Letters* 20: 1679–1682.